CFD Letters

Journal homepage:
https://semarakilmu.com.my/journals/index.php/CFD_Letters/index
ISSN: 2180-1363

Entropy Generation, Heat Transfer of Water Near Density Inversion Region with Relative Positions of Hot and Cold Walls: Numerical Analysis

Luan Nguyen Thanh[1,*], Phu Nguyen Minh[2], Ha Nguyen Minh[3]

[1] Faculty of Vehicle and Energy Engineering, Ho Chi Minh City University of Technology and Education (HCMUTE), Vietnam
[2] Faculty of Heat and Refrigeration Engineering, Industrial University of Ho Chi Minh City (IUH), Vietnam
[3] Faculty of Mechanical Engineering, University of Transport and Communications (UTC), Hanoi, Vietnam

ARTICLE INFO

Article history:
Received 27 January 2023
Received in revised form 25 February 2023
Accepted 23 March 2023
Available online 1 May 2023

Keywords:
Natural Convection; Density Inversion; Entropy Generation; Numerical Simulation

ABSTRACT

This study investigates the entropy generation and heat transfer of water density inversion region in a square cavity with the different relative positions of hot and cold walls by numerical simulation. Mathematical models are solved using the EES (Engineering Equation Solver) program. A physical model is a 38 mm square cavity filled with water, with cold and hot wall temperatures maintained at 0°C and 10°C. Results indicated that the Nusselt number of cases 1 (cold and hot walls on both sides) is higher than case 2 (hot wall above, cold wall below) and case 3 (cold wall above, hot wall below) by 1.582 and 1.059 times, respectively. The average total generation per unit volume in case 1 increases by 1.577 times and 1.059 times, respectively, compared to cases 2 and 3, which almost correspondingly increase with heat transfer capacity. Entropy generation by fluid friction is negligible.

1. Introduction

Natural convection is a form of heat transfer applied in many technical fields, such as refrigeration, insulation, and solar equipment. Many studies have focused on the natural convective properties of fluids. For water, the density of water has an unusual change at a temperature of 4°C. In this region, the convection mechanisms are complex; they strongly influence the temperature field and the convection flow. Natural convection of water near maximum-density region has been investigated in many studies. Michalek *et al.*, [1] tested four different numerical methods to determine a benchmark solution for natural convection in a square cavity. The result shows that the finite volume method with a sufficiently fine mesh size is the best option, and the temperature and velocity profile reference has been found. N. Seki *et al.*, [2] experimentally and numerically investigated a rectangular vessel filled with water. They reported that density inversion significantly influences natural convective heat transfer and the highest heat transfer corresponds to the dimension ratio of 0.8÷1.5. Lin and Nansteel [3] numerically investigated a water-filled square cavity. These authors found that the density distribution parameter significantly influences heat transfer,

* *Corresponding author.*
E-mail address: luannt@hcmute.edu.vn (Luan Nguyen Thanh)

https://doi.org/10.37934/cfdl.15.5.4253

and the high heat transfer with the density distribution parameter is less than or equal to 0.5. Hu *et al.*, [4] proposed and examined an annulus with a cylinder and an elliptical body inside. These researchers concluded that the higher Rayleigh number leads to the more potent the natural convection, and the elliptical body position does not affect the heat transfer. Li *et al.*, [5] analyzed an annulus with horizontal cylinders. They reported that the density distribution parameter, eccentricity, and Rayleigh number significantly influence the heat transfer process. Sivasankaran [6] conducted a numerical study of the wavy porous cavity with filled water. The findings suggest that the undulation and amplitude of the wavy wall significantly affect the heat transfer. Hossain and Rees [7] numerically examined a rectangular cavity with an internal heat source. They claim that the internal heat source significantly affects heat transfer, and the high heat source can change the flow direction. The above studies show that heat transfer properties of water near maximum density regions have been investigated by experiment and simulation in many different configurations.

Heat transfers are an irreversible process that leads to entropy generation. The entropy generation destroys the energy of the system. Thus, reducing entropy generation has been considered an optimum method for designing thermal systems [8, 9]. Some studies related to the entropy generation of water density inversion region can be found in previous literature. Phu and hap [10] investigated the entropy generation of a cavity with a circular and elliptical body inside. They reported the largest entropy generation for the cavity with the circular body and the smallest for the hollow cavity. Some studies related to nanofluid in the largest density regions can be found in studies by Kashani *et al.,* [11] Mahmoudi *et al.,* [12] Mirzaee and Lakzian [13].

Previous literature shows that heat transfer characteristic and entropy generation of the largest-density water region was investigated in different physical models. However, the specific assessment of entropy generation in the square cavity as the physical model suggested in studies [1, 3] with the different relative positions between the hot and cold surfaces has not been investigated. Thus, to provide more data on this issue, the Nusselt number, local heat transfer coefficient, and entropy generation were investigated by numerical simulation. The results can be referred for the actual heat transfer process, such as system thermal energy storage, movement of the ocean, ice forming, and ice melting.

2. Methodology

2.1 Mathematical Modeling

The entropy generation by heat transfer and fluid friction for the two-dimensional model can be determined [9, 14, 15]:

$$S_{gen,thermal} = \frac{k}{T^2}\left[\left(\frac{\partial T}{\partial x}\right)^2 + \left(\frac{\partial T}{\partial y}\right)^2\right] \quad (1)$$

$$S_{gen,friction} = \frac{\mu}{T}\left\{2\left[\left(\frac{\partial u_x}{\partial x}\right)^2 + \left(\frac{\partial u_y}{\partial y}\right)^2\right] + \left(\frac{\partial u_x}{\partial y} + \frac{\partial u_y}{\partial x}\right)^2\right\} \quad (2)$$

The total entropy generation is calculated as follows [9, 16]:

$$S_{gen,total} = S_{gen,thermal} + S_{gen,friction} \quad (3)$$

Average total entropy generation per unit volume [10]:

$$s_{gen,average} = \frac{1}{V}\int_V \left(s_{gen,thermal} + s_{gen,friction}\right)dV \quad (4)$$

where u_x, u_y, k ($Wm^{-1}K^{-1}$), V (m^3), $T(K)$ and μ ($kgm^{-1}s^{-1}$) are horizontal velocity, vertical velocity, thermal conductivity, volume of computational domain, temperature, and dynamic viscosity, respectively. The heat transfer rate can be determined [17]:

$$Q = hA(T_h - T_c) \quad (5)$$

where h ($Wm^{-2}K^{-1}$), $T_h(K)$, $T_c(K)$, and A (m^2) are natural convection heat transfer coefficient, temperature of hot and cold surface, and surface area, respectively. Nusselt number is calculated as follows [17]:

$$Nu = \frac{h.L}{k} \quad (6)$$

where $L(m)$ is distance between hot and cold wall. The local heat transfer coefficient is calculated by the formula [10, 17]:

x-axis direction: $h_{cb} = -k\frac{\partial T/\partial x}{(T_h - T_c)}$ (7)

y-axis direction: $h_{cb} = -k\frac{\partial T/\partial y}{(T_h - T_c)}$ (8)

2.2 Numerical Methodology

In this study, the physical model is a 38 mm square cavity filled with water at a pressure of 101325 Nm^{-2}, with cold and hot surface temperatures maintained at 0°C and 10°C. The relative positions of walls and boundary conditions are described in Figure 1.

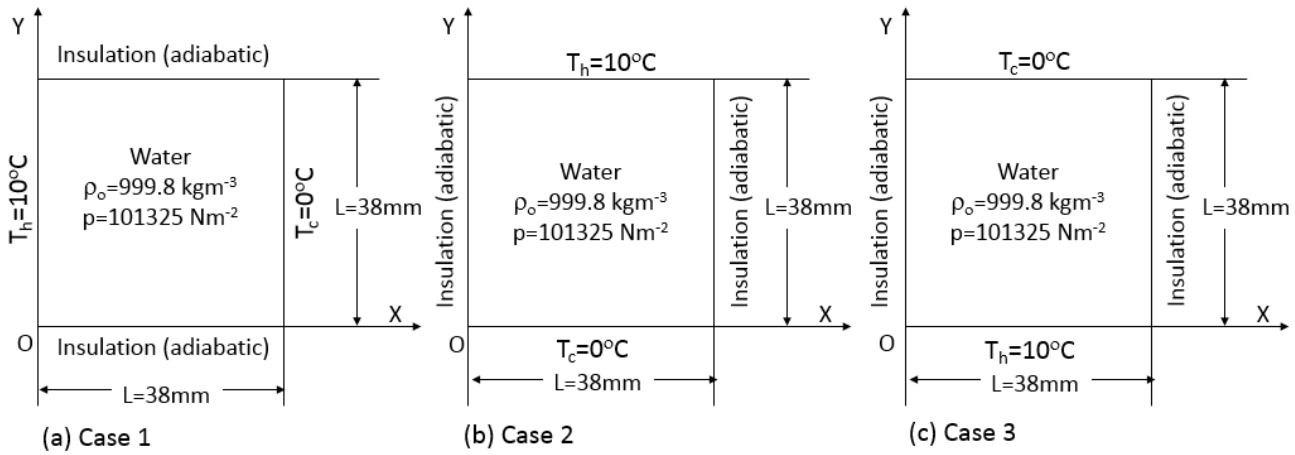

Fig. 1. Physical model and boundary conditions

It is detailed as follows:

Case 1: Cold and hot wall on both sides (Figure 1a)

$$T(x_o,y) = T_h, T(x_L,y) = T_c, x_o = 0, x_L = L \quad (9)$$

$$\frac{\partial T}{\partial y}(x,y_o) = \frac{\partial T}{\partial y}(x,y_L) = 0, y_o = 0, y_L = L \quad (10)$$

Case 2: Cold wall below, hot wall above (Figure 1b)

$$T(x,y_o) = T_c, T(x,y_L) = T_h, y_o = 0, y_L = L \quad (11)$$

$$\frac{\partial T}{\partial x}(x_o,y) = \frac{\partial T}{\partial x}(x_L,y) = 0, x_o = 0, x_L = L \quad (12)$$

Case 3: Cold wall above, hot wall below (Figure 1c)

$$T(x,y_o) = T_h, T(x,y_L) = T_c, y_o = 0, y_L = L \quad (13)$$

$$\frac{\partial T}{\partial x}(x_o,y) = \frac{\partial T}{\partial x}(x_L,y) = 0, x_o = 0, x_L = L \quad (14)$$

For simplicity of numerical analysis, the following assumptions are made: the incompressible fluid, two-dimension, unsteady form, and water density varies only in the buoyancy term. The equations governing can be summarized as follows [1, 3]:

Continuity:

$$\frac{\partial u_x}{\partial x} + \frac{\partial u_y}{\partial y} = 0 \quad (15)$$

Momentum:

$$\rho_o\left(\frac{\partial u_x}{\partial t} + u_x\frac{\partial u_x}{\partial x} + u_y\frac{\partial u_x}{\partial y}\right) = -\frac{\partial p}{\partial x} + \mu\Delta u_x \quad (16)$$

$$\rho_o\left(\frac{\partial u_y}{\partial t} + u_x\frac{\partial u_y}{\partial x} + u_y\frac{\partial u_y}{\partial y}\right) = -\frac{\partial p}{\partial y} + \mu\Delta u_y - g[\rho(T) - \rho_o] \quad (17)$$

Energy:

$$\frac{\partial T}{\partial t} + u_x\frac{\partial T}{\partial x} + u_y\frac{\partial T}{\partial y} = \alpha\Delta T \quad (18)$$

where x, *y, g, ρ, ρ$_o$, p, t,* and *α* (m^2s^{-1}) are dimensional horizontal coordinates, dimensional vertical coordinates, gravitational acceleration, density of fluid, reference density of fluid, pressure, time, and thermal diffusivity, respectively. The initial conditions are as follows [8,11]:

+ u=v=0 initial velocity of the water
+ ρ_o=999.8 kgm^{-3} is the reference density of water

The approach of false-transient was used to obtain a steady-state solution. Therefore, the above problem can be considered the steady form [1, 3]. This problem can be solved by ANSYS FLUENT with the setups as follows [1]:

i. Steady-state heat transfer.
ii. Equations governing were set up in the second-order-upwind scheme.
iii. The coupling velocity-pressure was conducted with the SIMPLE algorithm.
iv. Double precision was used to improve the accuracy of the result.

Figure 2 shows the mesh generation and mesh enhancement of the computational domain. Mesh sizes from 0.5 to 0.1 mm were performed to test the grid independence. A mesh size of 0.1 mm was chosen because the result was a good fit for the published literature [1] (Figure 3). Simultaneously, the results show the reliability of the present simulation. The turbulence model in this simulation is laminar [3]. The thermophysical properties of water are shown in Table 1, exported from EES software [18]. The residual equation of continuity, equation of energy, and velocity are 10^{-6}. In this study, dimensionless variables were used. The following dimensionless scales [1, 3, 19]:

Dimensionless horizontal coordinates: $X = x/x_L, x_L = L$ (19)
Dimensionless vertical coordinates: $Y = y/y_L, y_L = L$ (20)
Dimensionless horizontal velocities: $X_{velocity} = u_x.x_L/\alpha, x_L = L$ (21)
Dimensionless vertical velocities: $Y_{velocity} = u_y.y_L/\alpha, y_L = L$ (22)

Table 1
Thermophysical properties of water according to absolute temperature (K) [18]

No.	Property
1	Specific heat: c_p=4212 ($Jkg^{-1}K^{-1}$)
2	Density: ρ= -11289.1+164.178T-0.825887 T^2+0.00185663T^3-1.5762.10^{-6} T^4 (kgm^{-3})
3	Thermal conductivity: k=0.566 ($Wm^{-1}K^{-1}$)
4	Viscosity: μ=0.0017888 ($kgm^{-1}s^{-1}$)

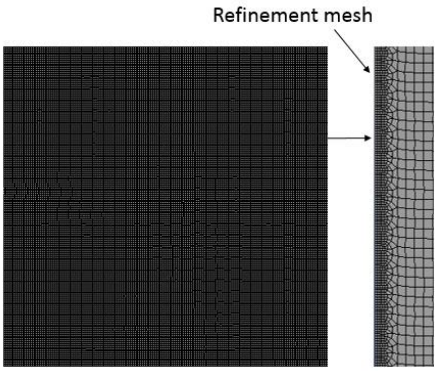

Fig. 2. Mesh generation and refinement mesh

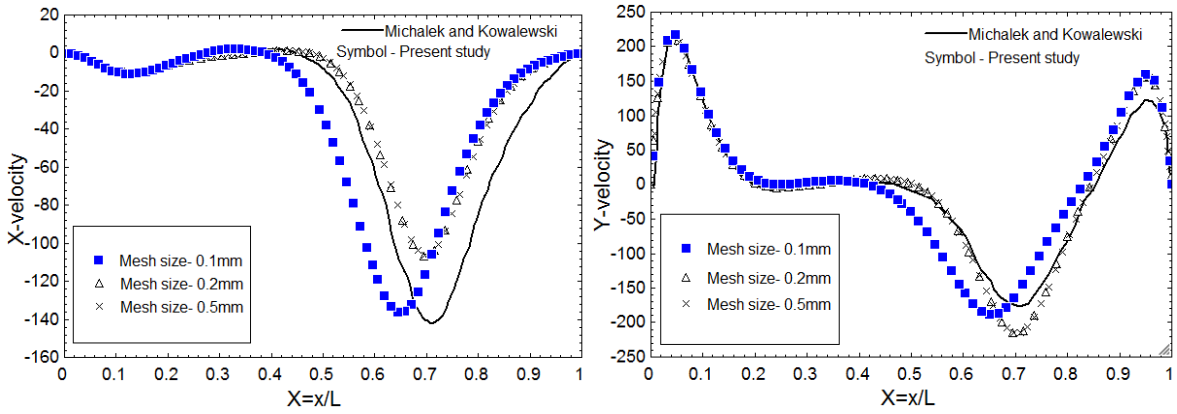

Fig. 3. Grid independence test and validation with previously published results [1]

3. Results

Figure 4 shows the temperature field, velocity distribution, and total entropy generation distribution of water in the square cavity corresponding to case 1. The results show that high-temperature water distributes close to the hot surface and top of the cavity; low-temperature water is concentrated near the cold surface and bottom of the cavity (Figure 4 (a)). The appearance of a temperature gradient leads to changes in the density distribution of the water, thus forming natural convection movement inside the cavity. The highest velocity of water in the cavity is 0.00085 ms-1; the high-velocity water flow is close to the heat exchange surfaces and the intersection of the two convection currents (see Figures 4 (b) and 4(c)).

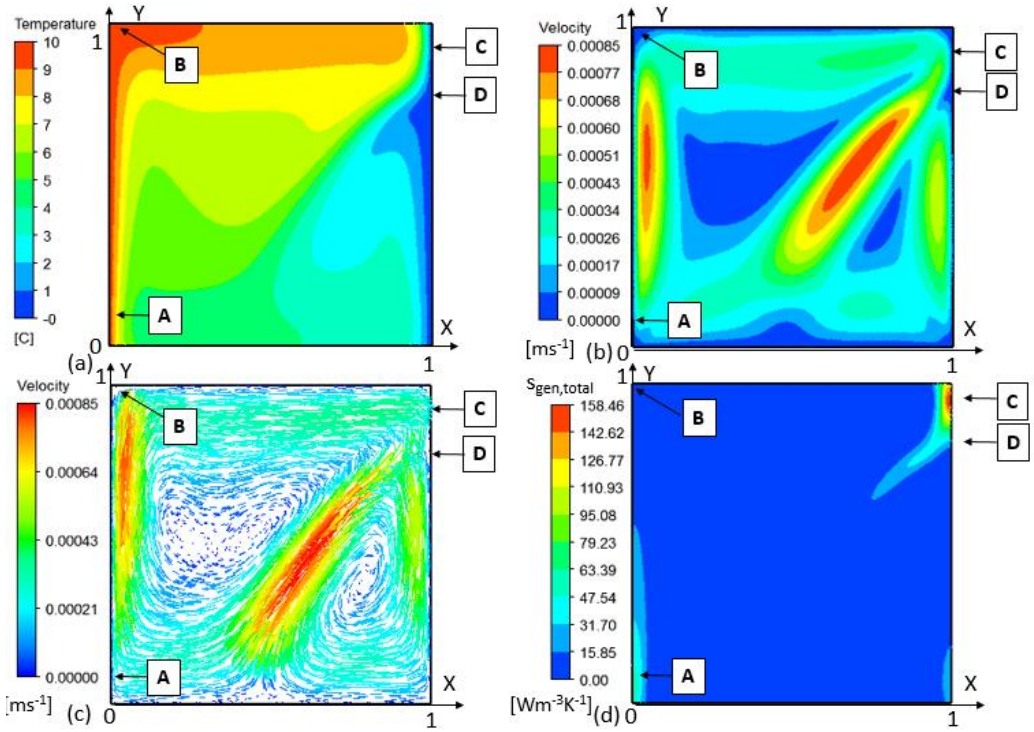

Fig. 4. Temperature (a), velocity magnitude (b), velocity vector (c), and total entropy generation (d) of case 1

Figure 5 shows the local heat transfer coefficient (LHTC) and local total entropy generation (LTEG) on the hot and cold surfaces of case 1. At Y = 0.04013 (point A) and Y = 0.9474 (point C), LHTC is the

largest and reaches 160.7 $Wm^{-2}K^{-1}$ and 259 $Wm^{-2}K^{-1}$, respectively (see Figure 5(a)). They are the re-attach point of convection current on the cold and hot surfaces, with high-velocity water and the high-temperature difference between the incoming water stream and the surfaces (see Figure 4), which leads to the highest heat transfer at those locations. Corresponding to those points, LTEG is the largest and reaches 56.94 $Wm^{-3}K^{-1}$ and 158.9 $Wm^{-3}K^{-1}$, respectively. It can be explained that: Along the hot wall, at point A, the water layers near the hot surface have a high-temperature difference; meanwhile, the thickness of the water layers is the smallest (see Figure 4(a), so the temperature gradient is the highest, leading to the entropy generation by heat transfer or total entropy generation is the highest at this location. The same explanation for point C on the cold wall. LHTC and LTEG are the smallest at Y=1 (point B) and Y=0.724 (point D). Those points have the slightest temperature gradient due to the water layers near surfaces having negligible temperature differences (see Figure 4(a)). Details of the local entropy generation along walls are indicated in Figure 5(b). The entropy generation by fluid friction is negligible due to the velocities of natural convection currents being small, with no appreciable difference between water near the surfaces and water far from it.

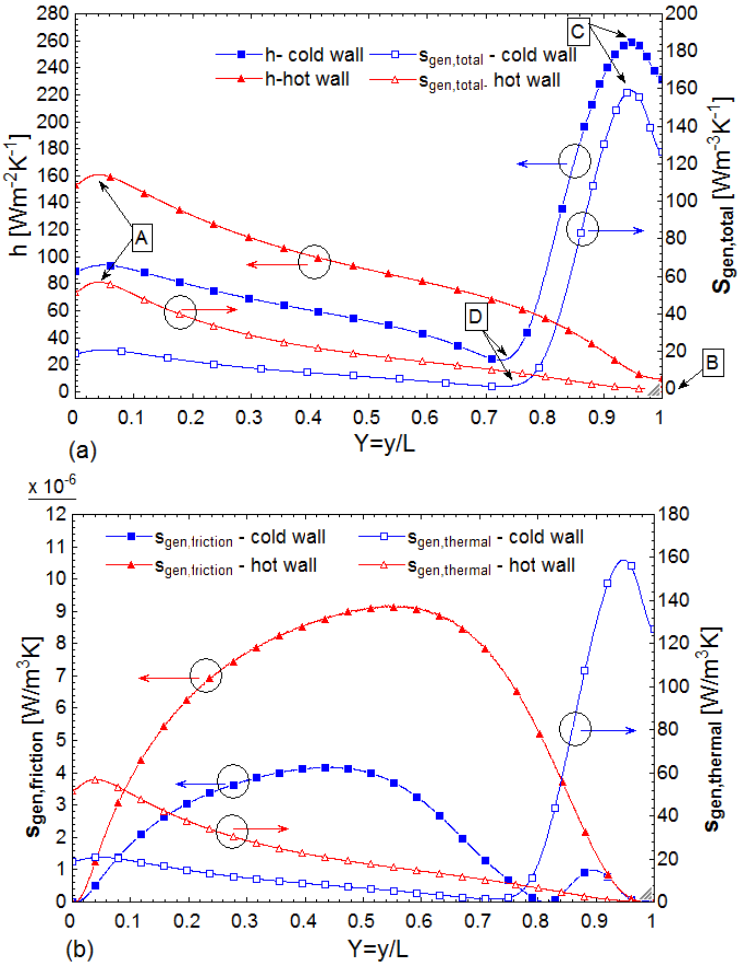

Fig. 5. Local heat transfer coefficient and entropy generation at hot and cold surfaces of case 1

The temperature field, velocity distribution, and total entropy generation of case 2 are shown in Figure 6. The temperature has stratification and symmetry (Figure 6(a)). The highest velocity of water in the cavity is 0.00073 ms^{-1}; the high-velocity water stream is near the left wall, right wall, and cavity center; the low-velocity water stream is close to the hot and cold surfaces (see Figure 6(b)). The cavity has two convection currents of equal size, and the contour of entropy generation has symmetry at

X=0.5 (see Figures 6(c), 6(d)). These symmetries may be due to the temperature stratification of the water layers from top to bottom. When the heat transfer process is stable, at the center region (X = 0.5), the water layers have a temperature of about 4°C (see Figure 6(a)), the highest density leads to the appearance of a water stream moving from top to bottom (under gravity), which creates the symmetries.

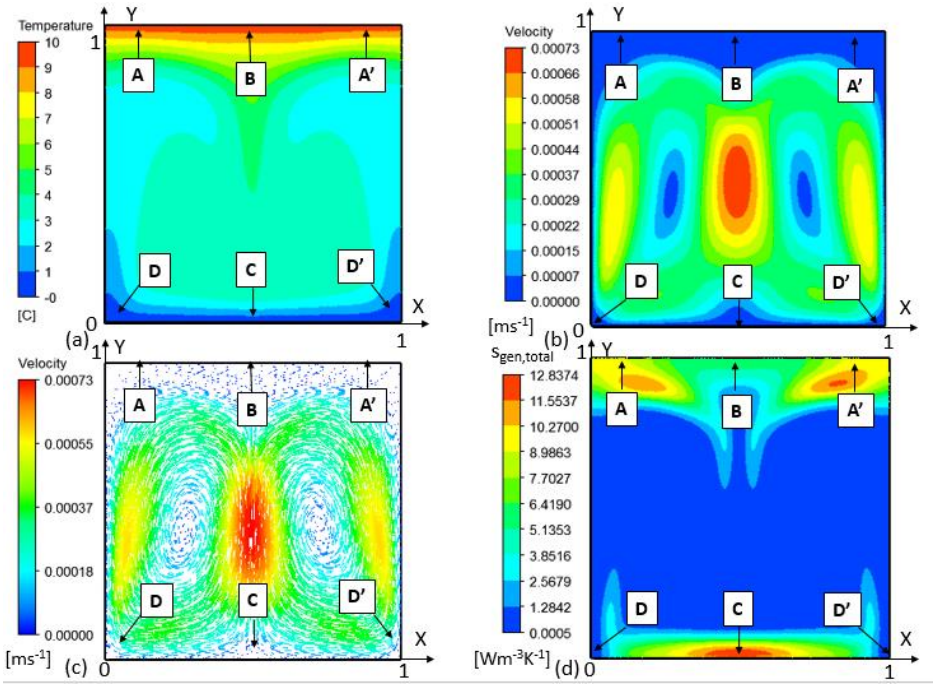

Fig. 6. Temperature (a), velocity magnitude (b), velocity vector (c), and total Entropy generation (d) of case 2

Figure 7 shows the distribution of LHTC and LTEG at hot and cold surfaces of case 2. At X = 0.06 and X = 0.94 (points A and A') and X=0.5 (point C), LHTC is the largest and reaches 66.7 $Wm^{-2}K^{-1}$ and 73.63 $Wm^{-2}K^{-1}$, respectively (see Figures 6, 7(a)). Corresponding to those points, LTEG is the largest and reaches 9.8 $Wm^{-3}K^{-1}$ and 12.84 $Wm^{-3}K^{-1}$, respectively. They are the re-attach point of convection current on the cold and hot surfaces, with high-velocity water and the high-temperature difference between the water flow and the surfaces. At X = 0 and X = 1 (points D and D') and X = 0.5 (point B), LHTC and LTEG are the smallest. These are points located at the corner and the region of the water stream leaves the hot surface, with low-velocity water and a slight temperature difference between the water flow and the surface (see Figures 6, 7(a)). Figure 7(b) shows local entropy generation along surfaces. The local entropy generation on the cold surface is more significant than on the hot surface. This trend is suitable for the cold surface location below. It results from the significant difference in temperature and velocity of water layers near the cold surface. The data lines are symmetric through the X=0.5 line, which perfectly agrees with the contour results in Figure 6(d).

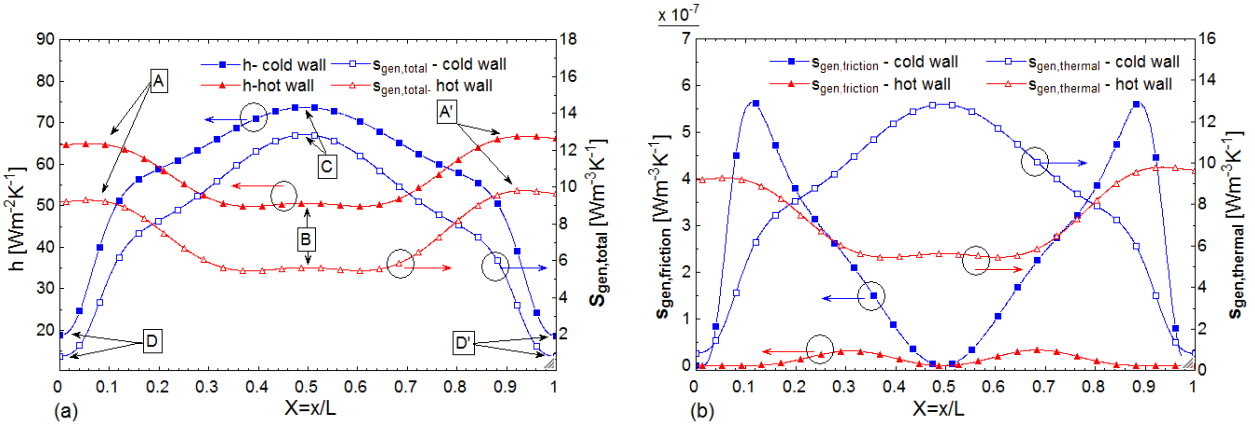

Fig. 7. Local heat transfer coefficient and entropy generation at hot and cold surfaces of case 2

Figure 8 describes the temperature field, velocity distribution, and total entropy generation distribution of case 3. The cavity has two convection currents of different sizes; the large convection current is deflected to the left (Figure 8(c)). This formation may be due to the unusual temperature field distribution, with the water layer having a temperature of about 4°C with the highest density in region X=2/3 line, even though the hot and cold walls are set perpendicular to the direction of gravity (see Figure 8(a)). The maximum velocity of water is about 0.00097 ms^{-1}. The region with the high velocity is near the left surface, the right surface, and the intersection of convection flows (Figures 8(b), 8(c)). The total entropy generation is the largest at re-attachment points (points A and C) on the walls (see Figure 8(d)).

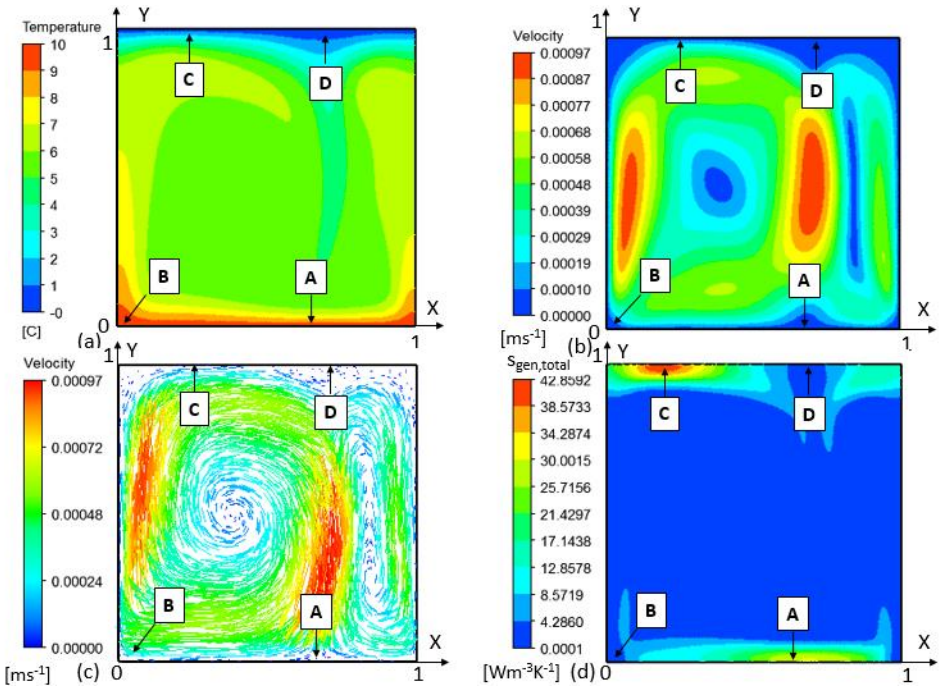

Fig. 8. Temperature (a), velocity magnitude (b), velocity vector (c), and total entropy generation (d) of case 3

Figure 9 shows the distribution of LHTC and LTEG at hot and cold surfaces of case 3. At X = 0.6842 (point A) and X = 0.1849 (point C), LHTC is the largest and reaches 117.4 Wm^{-2}K^{-1} and 134.5 Wm^{-2}K^{-1}, respectively (see Figures 8, 9(a)). These are points where the flow begins attachment to the wall with the highest velocity. Corresponding to those positions, LTEG is the largest and reaches about 30.37

$Wm^{-3}K^{-1}$ and 42.86 $Wm^{-3}K^{-1}$, respectively. At X=0 (point B) and X= 0.6776 (point D), LHTC and LTEG are the smallest. Those points are located at corners and the region where two convection currents leave the cold surface. Figure 9(b) shows detailed local entropy generation along the hot and cold surfaces, entropy variation along the walls is quite complex; it may result from forming two convection currents of different sizes in the survey domain.

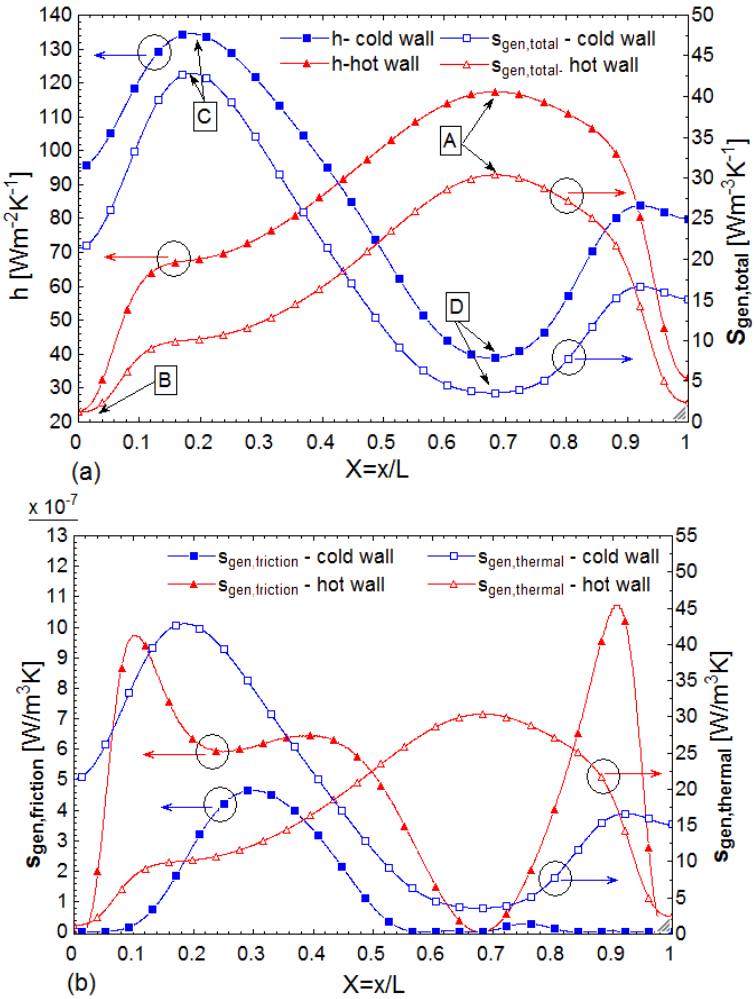

Fig. 9. Local heat transfer coefficient and entropy generation at hot and cold surfaces of case 3

Figure 10 compares the Nusselt number and the average total entropy generation per unit volume for the cases. Nusselt number of cases 1 is the largest, and Nusselt number of cases 3 is the smallest. Heat transfer of case 1 is higher than that of case 2 and case 3 by 1.582 and 1.059 times, respectively. The average total entropy generation of case 1 is higher than that of case 2 and case 3 by 1.577 and 1.059 times, respectively. The results show that the entropy generation almost correspondingly increases with heat transfer capacity, which is appropriate because the entropy generation due to friction is negligible in the survey cases.

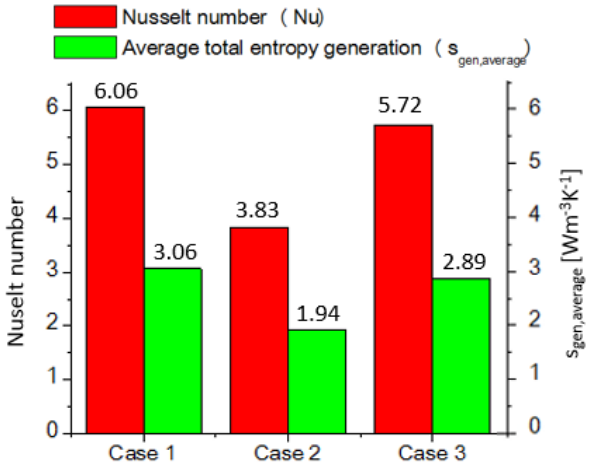

Fig. 10. Nusselt number and average total entropy generation per unit volume

4. Conclusions

This study investigated the entropy generation and heat transfer of water density inversion region in a square cavity with the different relative positions of hot and cold surfaces. Numerical analysis was performed on a two-dimensional model. The main findings are as follows:

i. Nusselt number of cases 1 (cold and hot walls on both sides) is higher than case 2 (cold wall below-hot wall above) and case 3 (cold wall above-hot wall below) by 1.582 and 1.059 times, respectively.
ii. The average total entropy generation per unit volume of case 1 is higher than case 2 and case 3 by 1.577 and 1.059 times, respectively. The entropy generation almost correspondingly increases with heat transfer capacity.
iii. Entropy generation by fluid friction is negligible.
iv. For case 1: The local heat transfer coefficient and local total entropy generation are the smallest at Y = 1 (hot surface) and Y = 0.724 (cold wall), which is the largest at Y = 0.04013 (hot wall) and Y = 0.9474 (cold wall).
v. For case 2: The local heat transfer coefficient and local total entropy generation are the smallest at X = 0.5 (cold wall) and X = 0.5 (hot wall), which is the largest at X = 0.06 and X = 0.94 (hot wall) and X = 0.5 (cold wall).
vi. For case 3: The local heat transfer coefficient and local total entropy generation are the smallest at X = 0 (hot wall) and X = 0.6776 (cold wall), which is the largest at X = 0.6842 (hot wall) and X = 0.1849 (cold wall).

Acknowledgement

This research is supported by Ho Chi Minh City University of Technology and Education (HCMUTE), Vietnam.

References

[1] Michalek, Tomasz, Tomasz A. Kowalewski, and Bozidar Sarler. "Natural convection for anomalous density variation of water: numerical benchmark." *Progress in Computational Fluid Dynamics, an International Journal* 5, no. 3-5 (2005): 158-170. https://doi.org/10.1504/PCFD.2005.006751

[2] Seki, N. "Free convective heat transfer with density inversion in a confined rectangular vessel." (1978). https://doi.org/10.1007/BF01805655

[3] Lin, D. S., and M. W. Nansteel. "Natural convection heat transfer in a square enclosure containing water near its density maximum." *International journal of heat and mass transfer* 30, no. 11 (1987): 2319-2329. https://doi.org/10.1016/0017-9310(87)90224-9
[4] Hu, Yu-Peng, You-Rong Li, Xiao-Feng Yuan, and Chun-Mei Wu. "Natural convection of cold water near its density maximum in an elliptical enclosure containing a coaxial cylinder." *International Journal of Heat and Mass Transfer* 60 (2013): 170-179. https://doi.org/10.1016/j.ijheatmasstransfer.2012.12.059
[5] Li, You-Rong, Xiao-Feng Yuan, Chun-Mei Wu, and Yu-Peng Hu. "Natural convection of water near its density maximum between horizontal cylinders." *International Journal of Heat and Mass Transfer* 54, no. 11-12 (2011): 2550-2559. https://doi.org/10.1016/j.ijheatmasstransfer.2011.02.006
[6] Sivasankaran, S. "Natural convection of cold water near its density maximum in a porous wavy cavity." *Flow and Transport in Subsurface Environment* (2018): 305-324. https://doi.org/10.1007/978-981-10-8773-8_10
[7] Hossain, Md Anwar, and DAS. Rees. "Natural convection flow of water near its density maximum in a rectangular enclosure having isothermal walls with heat generation." *Heat and mass transfer* 41 (2005): 367-374. https://doi.org/10.1007/s00231-004-0551-3
[8] Luan, Nguyen Thanh, and Nguyen Minh Ha. "Nghiên cứu đánh giá ảnh hưởng của thông số hình học và dòng chảy đến hiệu suất exergy của thiết bị trao đổi nhiệt ống lồng ống dạng xoắn bằng phương pháp mô phỏng CFD." *Journal of Technical Education Science* 63 (2021): 71-82. https://doi.org/10.54644/jte.63.2021.71
[9] Thanh Luan, Nguyen, and Nguyen Minh Phu. "Thermohydraulic Performance and Entropy Generation of Baffled Channel: Numerical Analysis and Optimization." *Journal of Thermophysics and Heat Transfer* 36, no. 2 (2022): 303-313. https://doi.org/10.2514/1.T6332
[10] Phu, Nguyen Minh, and Nguyen Van Hap. "Numerical Investigation of Natural Convection and Entropy Generation of Water near Density Inversion in a Cavity Having Circular and Elliptical Body." *Computational Overview of Fluid Structure Interaction* (2020): 121. https://doi.org//10.5772/intechopen.95301.
[11] Kashani, Sina, A. A. Ranjbar, Mohammad Mastiani, and Hooshyar Mirzaei. "Entropy generation and natural convection of nanoparticle-water mixture (nanofluid) near water density inversion in an enclosure with various patterns of vertical wavy walls." *Applied Mathematics and Computation* 226 (2014): 180-193. https://doi.org/10.1016/j.amc.2013.10.054
[12] Mahmoudi, Ahmed, Imen Mejri, Mohamed Ammar Abbassi, and Ahmed Omri. "Analysis of the entropy generation in a nanofluid-filled cavity in the presence of magnetic field and uniform heat generation/absorption." *Journal of Molecular Liquids* 198 (2014): 63-77. https://doi.org/10.1016/j.molliq.2014.07.010
[13] Mirzaee, Mahshid, and Esmail Lakzian. "Entropy generation analysis of eccentric cylinders pair sources on nanofluid natural convection with non-Boussinesq state." *Advanced Powder Technology* 28, no. 12 (2017): 3172-3183. https://doi.org/10.1016/j.apt.2017.09.034
[14] Kianpour, Ehsan, Nor Azwadi Che Sidik, Seyyed Muhammad Hossein Razavi Dehkordi, and Siti Nurul Akmal Yusof. "Numerical Simulation of Steady and Unsteady Flow and Entropy Generation by Nanofluid Within a Sinusoidal Channel." *Journal of Advanced Research in Fluid Mechanics and Thermal Sciences* 89, no. 2 (2022): 25-42. https://doi.org/10.37934/arfmts.89.2.2542
[15] Hussein, Ahmed Kadhim, Muhaiman Alawi Mahdi, and Obai Younis. "Numerical simulation of entropy generation of conjugate heat transfer in a porous cavity with finite walls and localized heat source." *Journal of Advanced Research in Fluid Mechanics and Thermal Sciences* 84, no. 2 (2021): 116-151. https://doi.org/10.37934/arfmts.84.2.116151
[16] Sidik, Nor Azwadi Che, Wan Mohd Arif Aziz Japar, and Yutaka Asako. "Entropy generation minimization in sinusoidal cavities-ribs microchannel heat sink via secondary channel geometry." *CFD Letters* 11, no. 7 (2019): 1-10.
[17] Cengel, Y., and Transfer Mass Heat. "A practical approach." *Heat and Mass Transfer* (2003).
[18] Klein, Sanford A., and F. Alvarado. "Engineering equation solver software (EES)." *F-Chart Software: Madison, WI, USA* (2013).
[19] Bouafia, Islam, Razli Mehdaoui, Syham Kadri, and Mohammed Elmir. "Conjugate natural convection in a square porous cavity filled with a nanofluid in the presence of two isothermal cylindrical sources." *Journal of Advanced Research in Fluid Mechanics and Thermal Sciences* 80, no. 1 (2021): 147-164. https://doi.org/10.37934/arfmts.80.1.147164